Proceedings of the 8th International Pipeline Conference
IPC2010
September 27 - October 1, 2010, Calgary, Alberta, Canada

IPC2010-31355

EDDY CURRENT SENSOR ARRAYS FOR PIPELINE INSPECTION WITH AND WITHOUT COATINGS

Andrew Washabaugh, Shayan Haque, David Jablonski, Neil J. Goldfine
JENTEK Sensors, Inc.
Waltham, MA, 02453-7013

ABSTRACT

Coatings are used on pipelines throughout the oil and gas industry for a variety of applications including corrosion protection, temperature maintenance, and weight control. These coatings also present a barrier to inspections for damage and typically need to be removed prior to inspection with nondestructive evaluation (NDE) methods. This has led to the development of improved NDE methods for detection and characterization of damage without removing the coatings or insulation.

This paper describes adaptations of JENTEK's Meandering Winding Magnetometer (MWM®)-Array technology for improved NDE in pipelines, including rapid and reliable imaging of damage, such as external corrosion, external mechanical damage, and stress corrosion cracking (SCC). The MWM-Array technology uses magnetic field-based sensor arrays and model-based inverse methods to determine electromagnetic and geometric properties of the pipeline material, which are then related to specific damage conditions of interest. This technology has been successfully applied in the aerospace and manufacturing industries and provides substantially improved performance for imaging surface and buried damage through coatings and for curved surfaces compared to conventional NDE methods.

Several representative applications are described. These include: 1) imaging of near surface material loss through moderate thickness coatings (less than 1.5-in. (38 mm)); 2) imaging of mechanical damage through thin (less than 0.25-in. (6.35 mm)) coatings; 3) imaging of SCC through very thin (less than 0.030-in. (0.76 mm)) and thin (less than 0.25-in. (6.35 mm)) coatings. For SCC, digital imaging of damage regions and automated analysis tools for assessing individual cracks has the potential to be a replacement for magnetic particle inspection (MPI). Initial work has demonstrated these capabilities in a laboratory environment with some field testing and ongoing work is transitioning this technology into field environments.

INTRODUCTION

Protective coatings are used on risers, piping, and pipelines throughout the oil and gas industry. However, these coatings act as a barrier to inspection and often need to be removed in order to inspect for damage with standard NDE. The damage can take a variety of forms, including internal and external corrosion, mechanical damage, and stress corrosion cracking (SCC), with corrosion under insulation a common form of damage. Although some NDE methods have been developed for imaging the pipeline through the protective coatings, these methods are typically too slow or require expensive scanners to be used in practical applications. This has led to the need for reliable and lower cost solutions for high resolution imaging of damage from outside the pipeline through coatings. In addition, even after the coatings are removed, it is beneficial to be able to both image and characterize the damage without the coatings.

A wide variety of these protective coatings are in use. Fusion bonded epoxy (FBE) and other coatings are routinely applied to oil and gas pipelines to prevent contact of the steel with corrosive soil, bacterial, fungal, and moisture environments, with FBE currently the most widely used coating system. An abrasion resistant overcoat is usually applied on top of the first layer of FBE for increased resistance to mechanical damage. Other coating systems that are widely used in pipelines, especially older pipelines, include polyethylene wrap, coal tar enamel, or an enamel tape wrap. Coating methods are often combined. Overall coating thicknesses range from approximately 0.010-in. (0.25 mm) for FBE and polyethylene coatings to 0.25-0.50 in. (6.35-12.7 mm) for the older coal tar coatings. Insulation is typically a dielectric (electrically and thermally insulating) material up to approximately 4.-in (10 cm) thick that in turn can be surrounded by a metallic foil layer.

This paper describes adaptations of JENTEK's Meandering Winding Magnetometer (MWM®)-Array technology for providing improved NDE of pipelines. This

technology has been successfully applied in the aerospace and manufacturing industries and provides substantially improved performance for imaging surface and buried damage through coatings and for curved surfaces compared to conventional NDE methods. [1-5]

BACKGROUND ON MWM-ARRAY TECHNOLOGY

MWM and MWM-Arrays are inductive, eddy-current-based sensors that are conformable and provide inspection and monitoring capabilities for conducting materials, such as steel pipeline walls and drill pipe. [6] As shown in Figure 1, the original MWM sensor geometry had a meandering primary winding for creating a spatially periodic magnetic field when driven by an electrical current – hence the MWM name. Secondary windings (sense elements) are located on opposite sides of the primary for sensing the response.

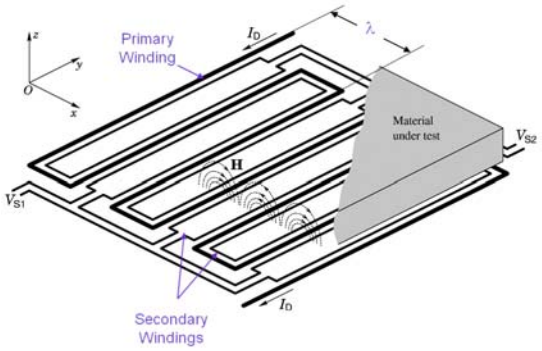

Figure 1. Original MWM sensor geometry [6].

Printed circuit microfabrication techniques are typically employed to produce the sensors, resulting in highly reproducible (i.e., essentially identical) sensors. By fabricating the windings on thin and flexible substrate, a conformable sensor can be produced. These thin and conformable sensors can be scanned across a surface, mounted on an exposed surface, or embedded within or between coating/pipeline layers or under an overwrap or repair. The relatively simple layout for the windings permits operation over a wide frequency range, typically between 1 kHz and 40 MHz. For inspection through steel pipeline walls, for example for internal corrosion inspection from the outside, a lower frequency capability (<100 Hz) is also being developed.

Note that the depth of penetration of the magnetic field into the test material depends upon both the input current frequency and sensor geometry (drive winding spatial wavelength λ) as shown in Figure 2. The penetration depth is limited by the skin depth at high frequencies and by the sensor geometry at low frequencies. At low frequencies the magnetic fields from a larger spatial wavelength sensor will penetrate further into the material under test than a shorter spatial wavelength sensor. (Note that the spatial wavelength λ of Figure 1 indicates the spatial periodicity for the drive; for the MWM-Arrays of Figure 3 the relevant dimension is the gap between the drive and sense element and which is defined as λ/4.) Thus, while small sensor arrays can be used to create high spatial resolution property images, large sensor arrays are required for inspecting through thick materials, either steels, coatings, or insulation. For bare metal or very thin coatings, very high resolution imaging is achieved with the FA28 MWM-Array of Figure 3(a). The FA24 MWM-Array shown in Figure 3(b) has larger dimensions than that of the FA28 and permits inspection through thin coatings. The VWA001 MWM-Array shown in Figure 3(c) has a variable spatial wavelength, where the distance between the drive winding and sense element can be adjusted, which enables both deep penetration and relatively high resolution compared to other typical low frequency eddy current methods.

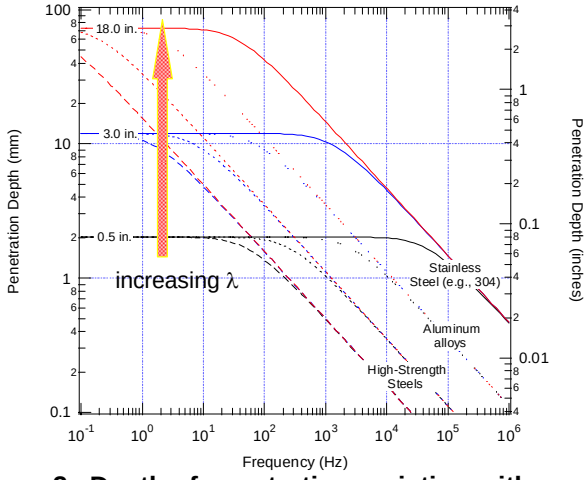

Figure 2. Depth of penetration variation with sensor dimension.

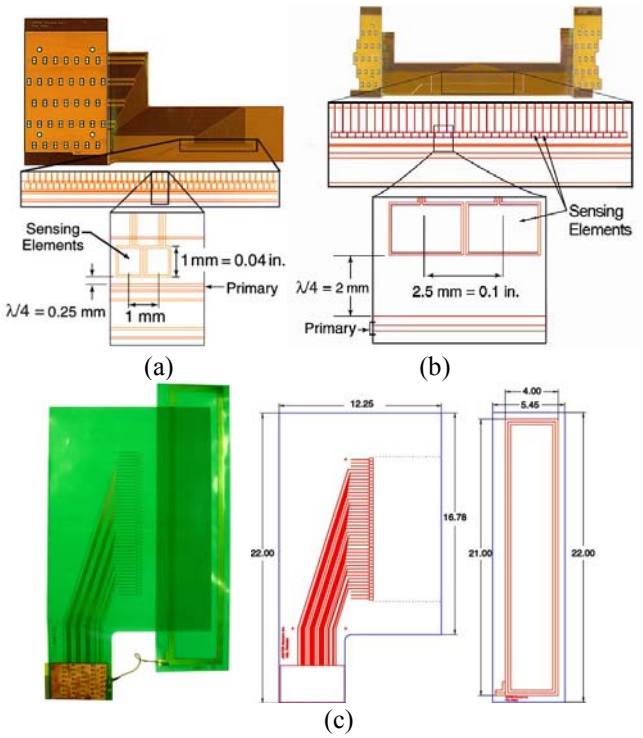

Figure 3. Several MWM-Arrays: (a) FA28; (b) FA24; and (c) VWA001 [6].

MWM and MWM-Array responses are converted into material or geometric properties using measurement grids [7]. These grids convert two known values, such as the magnitude and phase (or real and imaginary parts) of the transimpedance, into the unknown properties of interest, such as electrical conductivity, magnetic permeability and lift-off. The grids are generated using a forward model and properties of the test material to create two-dimensional databases, or precomputed responses, which can be displayed graphically to support procedure development. Figure 4 shows a conductivity/lift-off grid and data from one channel of an MWM-Array in scans performed with four different insulating coating (shim) thicknesses. This figure illustrates how the conductivity and lift-off (representing the total thickness of the insulating layers) can be independently measured. For magnetizable steels, the magnetic permeability is often determined, which in turn is related to the material microstructure and the residual or applied stress at a given location. Higher-order databases are used for the determination of more than two unknown properties of interest, such as coating thickness (via sensor lift-off or proximity), metal wall thickness, and metal electrical conductivity and/or magnetic permeability.

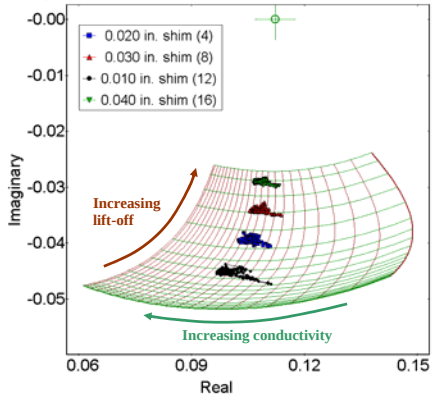

Figure 4: Representative measurement grid [6].

EXTERNAL CORROSION IMAGING

MWM-Arrays that use a single drive winding and multiple sense elements are well-suited to rapid imaging of material loss through coatings [6]. Small sensor array geometries can be selected for creating high spatial resolution images of the damage areas through thin coatings while larger sensor geometries are required for imaging through thicker coatings.

This imaging capability has been demonstrated on a 6.625-in. diameter, 4 ft long pipe section that had a wall thickness of 0.28-in. and machined flaws on the external surface. Figure 5 shows property images obtained for the FA24 MWM-Array at a frequency of 100 kHz. The left and bottom axes are expressed in inches. The regions of material loss are clearly visible as areas of increased lift-off as the effective distance between the sensor array and the steel surface increases. The shapes of the regions are also appropriate; for the shallower and larger flaws the regions are rectangular in shape. The flaw regions are also apparent in the relative permeability image. Since the magnetic permeability can vary with material condition, such as residual stress, this may reflect property changes associated with the flaw machining process. Here, plastic sheets are wrapped around the pipe section to simulate the presence of a very thin (0.020-in. thick) insulating coating. An air-shunt calibration was performed. This type of calibration uses a measurement in air and a measurement with a shunt sensor in which the sense elements are shorted. This is a robust method of calibration since it does not rely on knowledge of a reference material, but it requires having a shunt that is essentially identical to the sensor array. Figure 6 shows B-scan (individual sense element response) plots of the lift-off response for a sense element that passed over the center of each region. These plots show that each of the material loss regions is detected.

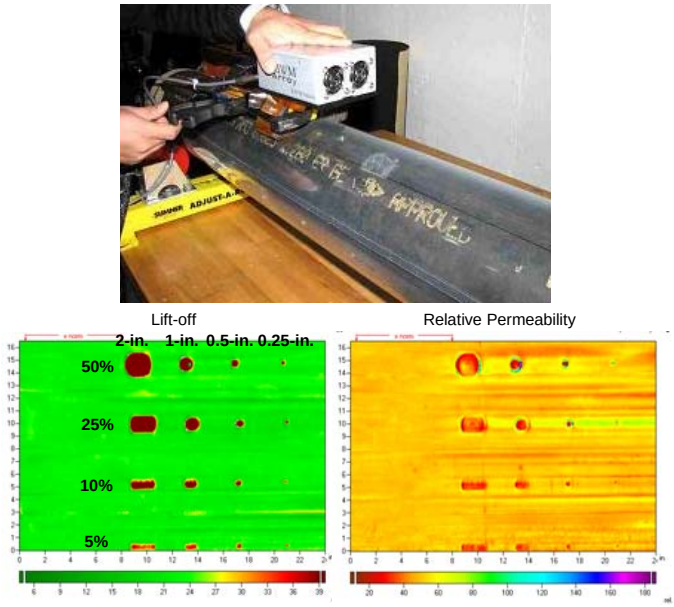

Figure 5. (Upper) Photograph of an FA24 MWM-Array being scanned over a pipe section with a thin coating. (Lower) Effective property images showing flaws machined in the outside surface.

Measurements were also performed with a large MWM-Array, the VWA001, as shown in Figure 7. This array has a 0.56 m (22-in.) long drive winding and a linear array of sense elements fabricated separately so that the spatial wavelength (or the distance between the drive winding and sense elements) could be selected based on the nominal coating on the test article. In this case, 12.7 mm (0.5-in.) thick Neoprene was wrapped around the pipe section and a drive-sense gap of 25.4 mm (1.0-in.) was selected. The prototype wrap-around scanner fixture has a linear position encoder at the front and two support wheels in the back. The plastic sheet holds the sensor in place and attaches to the scanner fixture on each side. Figure 7 shows scan results and small areas of material loss are clearly visible.

Figure 8 shows lift-off images obtained with the VWA001 for some thicker coatings. The images show the 25% and 50% material loss regions, with the high spatial resolution images obtained for coating thicknesses less than around 1.0-in. For thicker coatings the larger flaws are still visible but there is a noticeable degradation of the flaw images.

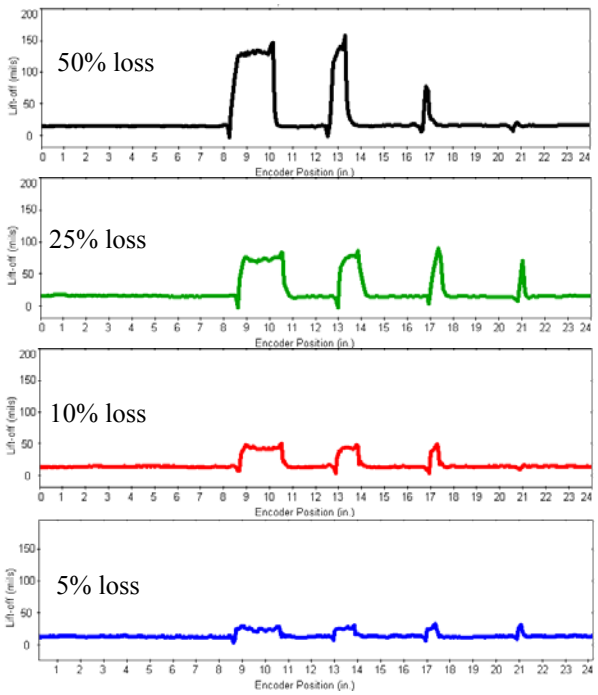

Figure 6. B-scan lift-off plots over material loss regions for an FA24 with a 0.020-in. thick coating.

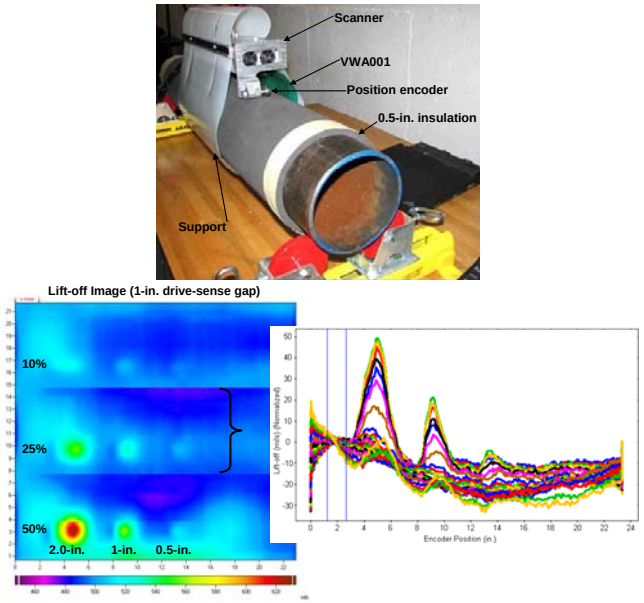

Figure 7. (Upper) VWA001 MWM-Array and prototype wrap-around fixture over a pipe section with a medium thickness coating. (Lower) Scan results showing material loss regions for a 0.5-in. coating.

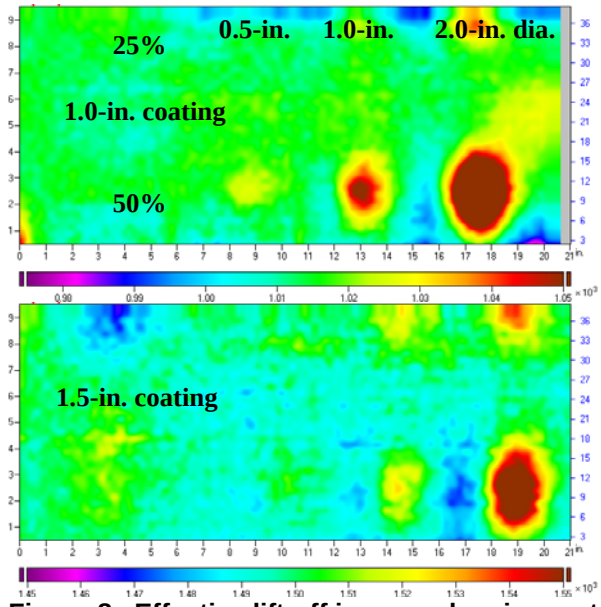

Figure 8. Effective lift-off images showing material loss regions through 1.0 and 1.5-in. coatings.

Measurements have also been performed on 40 ft long, 6.-in. diameter riser sections made available by Chevron and PRCI (Pipeline Research Council International). Figure 9 shows five sections containing embedded defects with each section having a 0.5-in. thick "Splashtron" coating, along with the prototype external scanner fixture and VWA001. Since each scan spanned approximately ¼ of the pipe, scans were made at four positions around the circumference to construct a complete scan image. Figure 10 through Figure 12 show initial results over several detected flaws in the pipe underneath the coating. These are absolute images, where the impedance measurement data has been processed to obtain the lift-off (proximity of each sense element to the steel pipe surface) and the relative permeability for the steel pipe wall (which is related to material property and residual stress). Flaw responses are evident in each of these images and appear as a local increase in lift-off and variation in magnetic permeability; variations in lift-off that are not associated with a change in the magnetic permeability are caused by coating thickness variations. Note that no attempt was made to filter these images to reduce channel-to-channel variability of the images at this time.

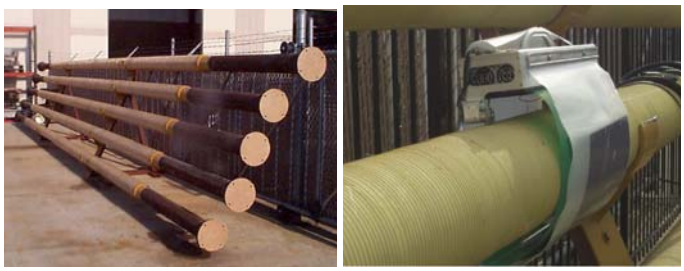

Figure 9. (Left) Simulated PRCI riser samples with embedded corrosion defects. (Right) Photograph of a prototype external scanner on these pipe sections.

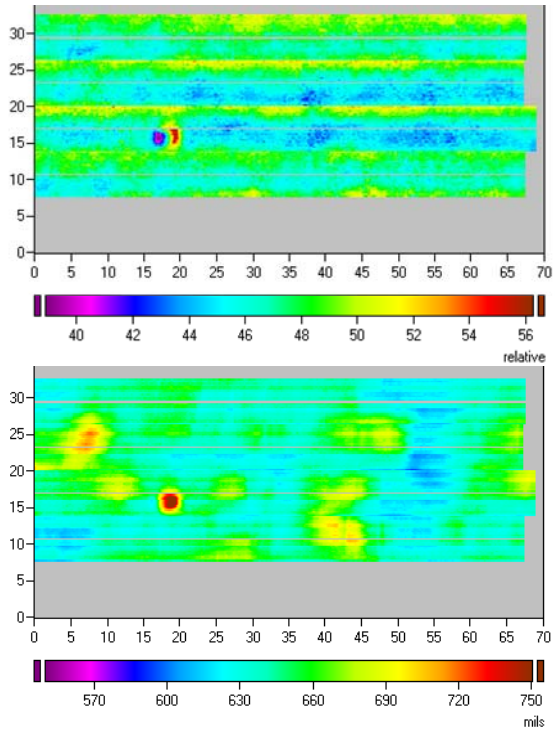

Figure 10. Property images for an elongated flaw: (Upper) Relative permeability; (Lower) Lift-off.

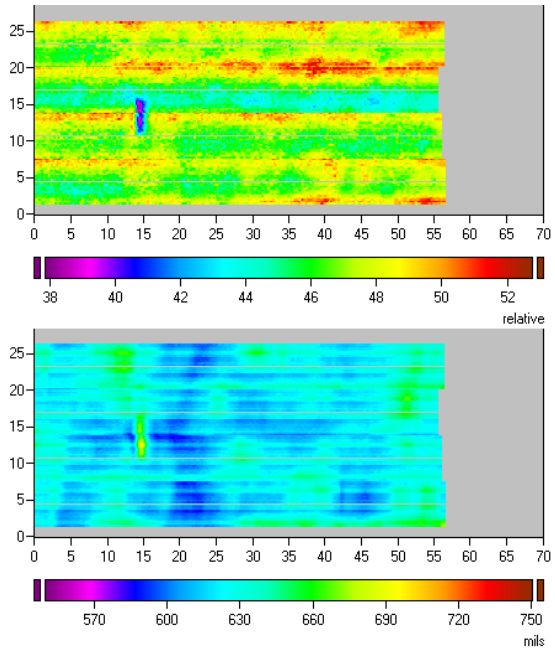

Figure 11. Property images for a circumferential flaw: (Upper) Relative permeability; (Lower) Lift-off.

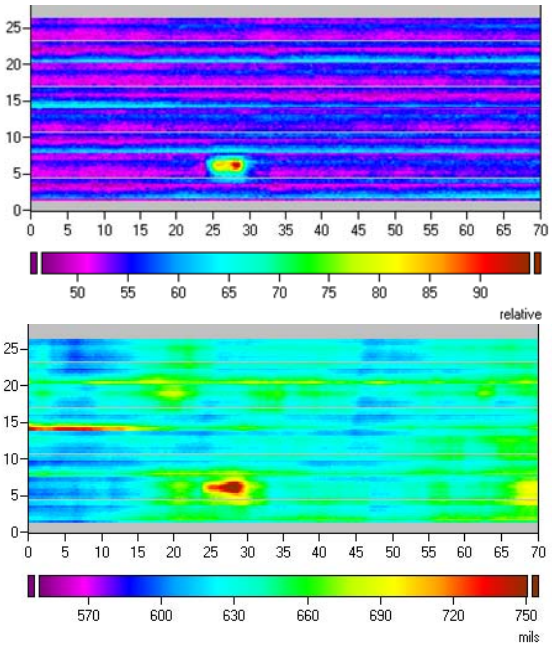

Figure 12. Property images for an axial flaw: (Upper) Relative permeability; (Lower) Lift-off.

MECHANICAL DAMAGE IMAGING

Several measurements have shown that the MWM-Arrays can image mechanical damage in steel. These measurements involve scanning an MWM-Array over the surface, processing the data with measurement grids to obtain lift-off (sensor proximity) and permeability images of the material being inspected, and evaluating these images to determine the presence and extent of the damage. Mechanical damage appears as both an increase in sensor proximity, i.e., lift-off (associated with denting or gouging of the surface), and a variation in the local magnetic permeability (which is associated with variations in the residual stress around the damage site and other microstructure changes due to plastic deformation).

As an example, measurements were performed on a 16-in. diameter pipeline section at RTD that included seven discrete regions of mechanical damage. The damage regions consisted of a combination of dents and gouges and the severity of the damage varied in shape and size. Figure 13 shows the pipeline section with highlighted mechanical damage regions. A single axial scan, covering six damage sites, was performed with an FA26 sensor and a standard manual scanning cart. Figure 13 also shows property images. A 0.010-in. thick plastic sheet was placed over the pipe surface to protect the sensors and to simulate the presence of a thin coating layer. Note that only six of the damage sites are shown on the property images since the seventh was close to the edge of the pipeline section. The markers on the pipeline section only appear in the lift-off images, not the permeability, indicating that the permeability and lift-off values are estimated independently. Figure 14 shows an expanded view of the effective property images for

one of the damage locations. As with the dented plate measurements, the mechanical damage appears as both a change in the lift-off and a change in the relative permeability. This shows that high spatial resolution images are readily obtained for mechanical damage sites; ongoing work is aimed at using this NDE information to characterize the damage.

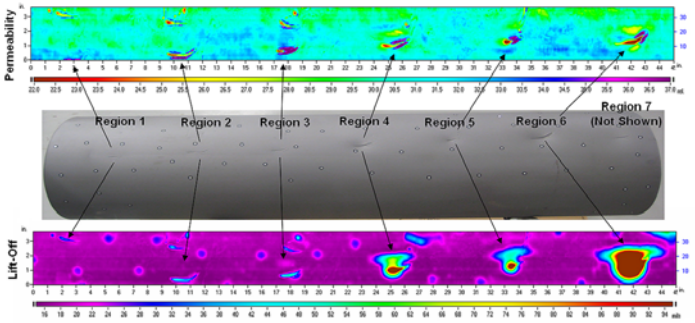

Figure 13. A 5-ft long, 16-in. diameter pipeline section with seven regions of mechanical damage as well as complete FA24 axial scan images of permeability (top) and lift-off (bottom).

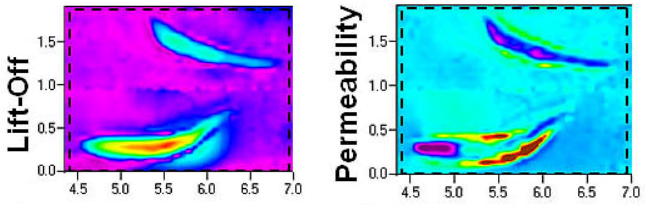

Figure 14. Expanded effective property images for one of the damage regions from Figure 13.

Additional measurements have been performed on steel plates to help develop a better understanding of the relation between the effective property measurements and the mechanical damage conditions. For example, consider the steel plate of Figure 15. The depressed area is clearly indicated in the lift-off scans. A hydraulic press was used to introduce a dent into the center of the steel plate. The 1-in. diameter punch created a shallow (0.100 in.), flat-bottomed depression, surrounded by a depressed region. The plate was scanned using the FA24 MWM-Array. The resulting lift-off and permeability images and plots are shown in Figure 16. The depressed area is clearly indicated in the lift-off scans. In addition, the permeability scans indicate an area of residual stress surrounding the depressed area.

Additional measurements have been performed on 0.25-in. thick steel plates that were indented with steel balls. The steel balls had a diameter of 0.782-in. or 1.575-in. Figure 17 shows comparisons between lift-off measurements along the center-line of the dent to measurements made with a dial indicator. The raw measured lift-off shape is similar to the dial indicator but less than the dial indicator depth because the measurement grids used here assumed uniform planar layers. Since the dented surface is curved, the planar models are not as accurate; other analysis tools were used to determine a scaling factor correction that compensates for the geometric effect on the dent profile estimate. For a shallow dent, the correction factor is near one. However, for deep and narrow dents, the correction factor can be significant. These model-derived scale factors match those obtained empirically and confirm that accurate dent depth and geometry can be made using MWM-Arrays when corrected for the non-planar geometry that occurs in a steel wall with mechanical damage.

Figure 15. Left: A dented steel plate. Right: Plate with an FA24 MWM-Array and a 0.020-in. plastic sheet.

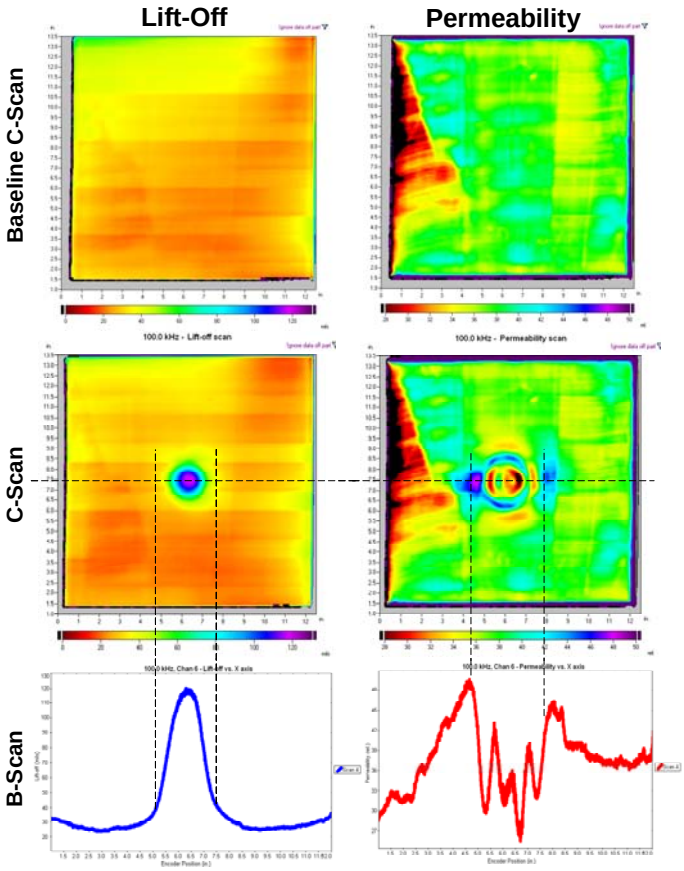

Figure 16. Top Row: Baseline scan images. Middle and bottom rows: Images and B-Scans of lift-off (left) and permeability (right) across the plate of Figure 15.

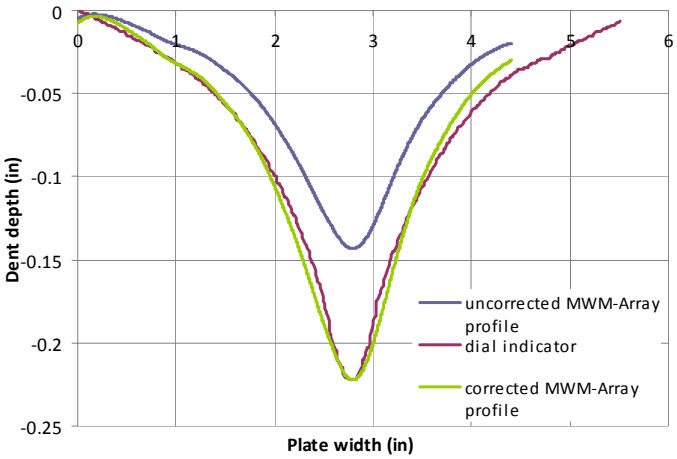

Figure 17. Comparison between lift-off and dial indicator measurements.

The geometry of the MWM-Array leads to directional sensitivity of the sensor array so that scans with perpendicular orientations provide complimentary information about the material properties of the test material. For example, the MWM-Array is sensitive to the magnetic permeability in a direction perpendicular to the drive windings. Thus, when scanning over a circular feature as in Figure 16 the magnetic permeability appears asymmetric since only the component of the magnetic permeability perpendicular to the sensor array is observed. However, if the feature is scanned in two orientations, as illustrated in Figure 18, then both components are observed.

Figure 19 shows three images of a circular mechanical damage site. The image on the left and center are images of the magnetic permeability in the perpendicular and parallel directions. The image on the right is the summation of these two images (at each pixel), providing a measure of the residual stress at that location. A relative increase in the magnetic permeability for this material represents an increase in tensile stresses (or an increase in susceptibility to stress corrosion cracking or fatigue crack initiation and growth). Note that this data was taken through a 0.03-in. insulating layer. Figure 20 shows the lift-off which provides the surface topology (*magnetic profilometry*), images corresponding to the same perpendicular, parallel and summed images as in Figure 19. The lift-off images are the same which indicates that the Grid Methods are independently providing permeability and lift-off values.

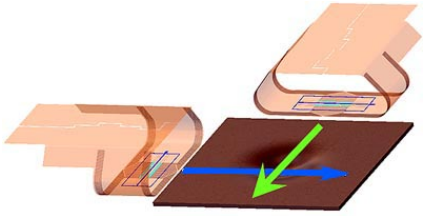

Figure 18. Illustration of the MWM-Array drive winding orientation during scanning.

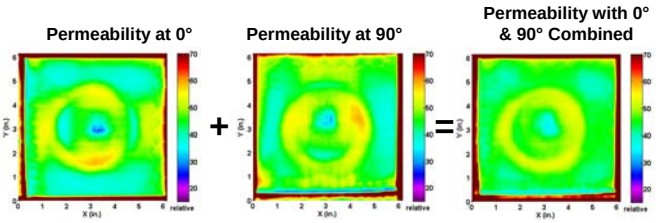

Figure 19. Images of a circular mechanical damage site. Summing the images from two perpendicular orientations yields an improved image.

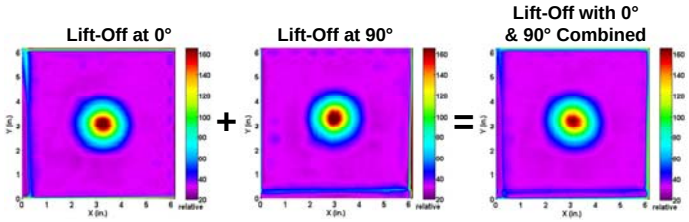

Figure 20. Lift-off images corresponding to the permeability images of Figure 19.

Figure 21 provides an interesting visualization of these results. The JENTEK grid methods provide imaging of the surface topology and, at the same time in the same scan, imaging of the magnetic permeability (or residual stress pattern). As shown in Figure 21(left), the surface topology is extremely smooth as intended, but, as shown in Figure 21(right), the residual stresses are highly varied. Further examination of the manner in which the dents were made suggested that gripping the part close to the indentation prevented a smooth transition of the residual stresses, producing the more jagged response shown in the permeability image.

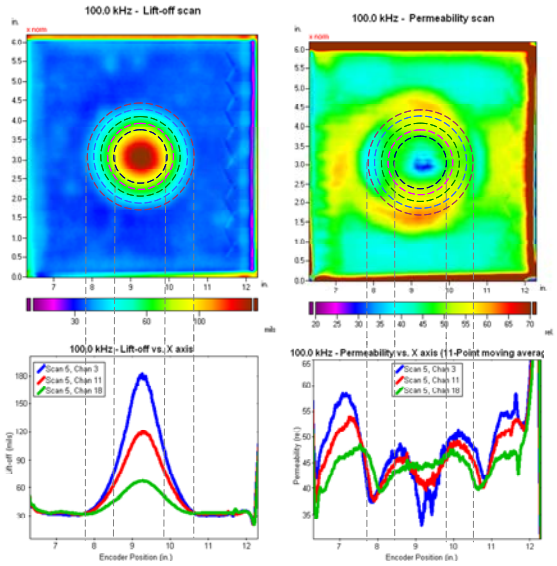

Figure 21. Independent imaging of the surface topology and magnetic permeability at the same time in the same scan: (Left) Lift-off (surface topology); (Right) Magnetic permeability.

Figure 22 shows effective permeability images for one of the plates before and after annealing. The left and middle images were obtained by averaging the measured permeabilities in two orientations, which reflects the symmetrical circular shape of the dent. The difference was found by subtracting the permeability images before and after annealing; since annealing should remove the residual stress, these results indicate that the permeability measurements are sensitive to the stress distribution around the mechanical damage.

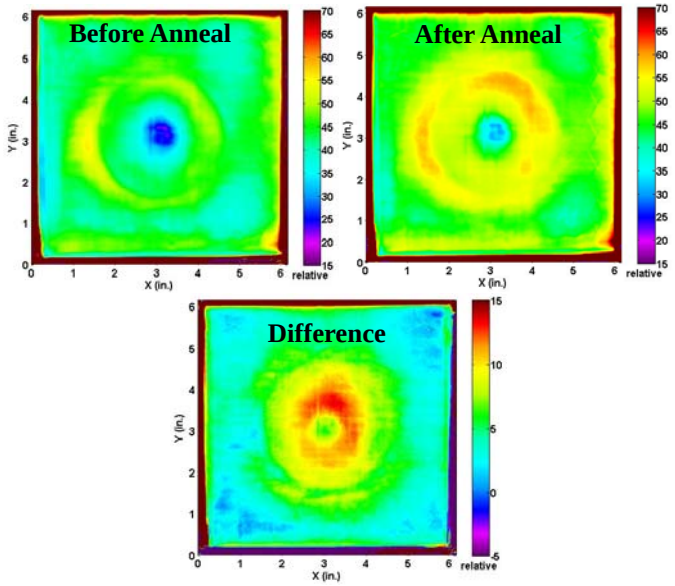

Figure 22. Effective permeability images for symmetric mechanical damage in a plate.

SCC IMAGING THROUGH THIN COATINGS

A variety of measurements have been performed on steel pipeline sections that contain region of SCC to demonstrate the capability to image SCC through thin and medium-thickness coatings. One pipeline section, provided by RTD, is approximately triangular in shape as shown in Figure 23(upper) along with a hand-scanner. This section has approximate dimensions of 18-in. by 13-in. and is 0.33-in. thick. An MWM-Array is located at the bottom of the scanner and supported with a layer of foam so that the sensor array conforms to the surface of the section. Results of FA28 (very small size MWM-Array) scans are presented in Figure 23 (middle and lower). The square patch visible in the lift-off image is paper to simulate a very thin coating variation. The fact that the square shows up in the lift-off image only, and not in the conductivity image, illustrates that the multivariate inverse methods are effectively compensating the conductivity measurement for uncontrolled variations in lift-off. The fact that crack-like conductivity responses are present in the area covered by the paper (as well as the areas not covered) illustrates that SCC can be detected and accurately imaged through a very thin coating.

Figure 24 shows a series of conductivity scan images obtained with an FA24 (small-size) MWM-Array over coating thicknesses ranging from 0.010-in. to 0.260-in. The region of SCC damage appears as a reduction in the electrical conductivity and is apparent on the left side of the images. For coatings less than approximately 0.080-in. in thickness, the images show individual cracks within the SCC clusters. However, as the coating thickness gets larger the responses from nearby cracks overlap and it is more difficult to resolve individual cracks. The SCC clusters remain visible with this sensor array even for thicker coatings with thicknesses of order 0.25-in.

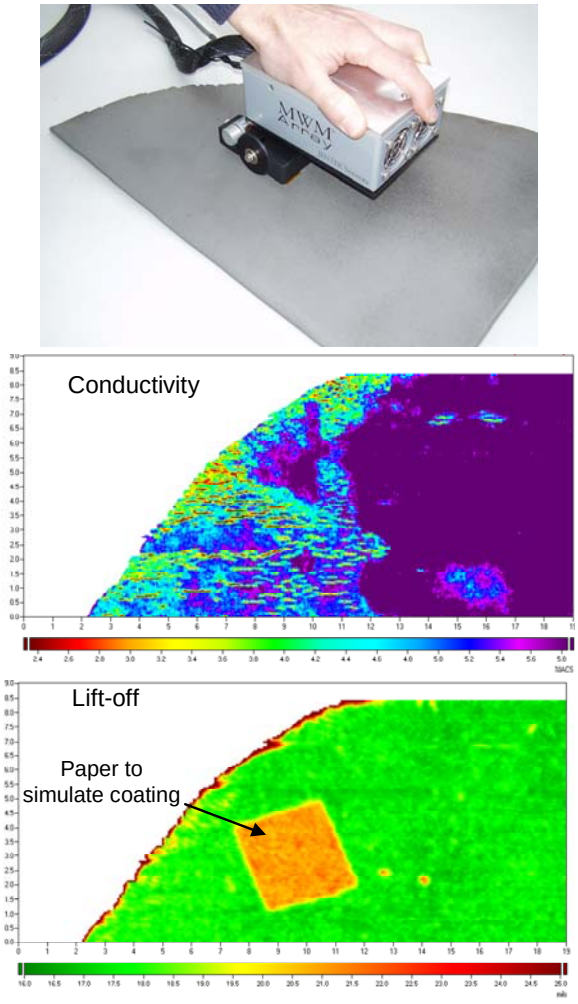

Figure 23. (Upper) Photograph of a steel pipeline section having clusters of SCC damage with a hand-scanner. Effective property images for conductivity (middle) and lift-off (lower) from an FA28.

Signal processing algorithms for automated determination of crack length and crack spacing have also been developed. An example of the crack sizing algorithm uses FA28 data similar to that shown in Figure 23. Figure 25(left) shows all indications that are large enough to be called discrete cracks.

Figure 25 (right) shows in yellow those cracks that meet the criteria for "interacting cracks" with the crack shown in brown. Prescribed repair actions are based upon the dimensions of the largest interacting crack in an SCC colony.

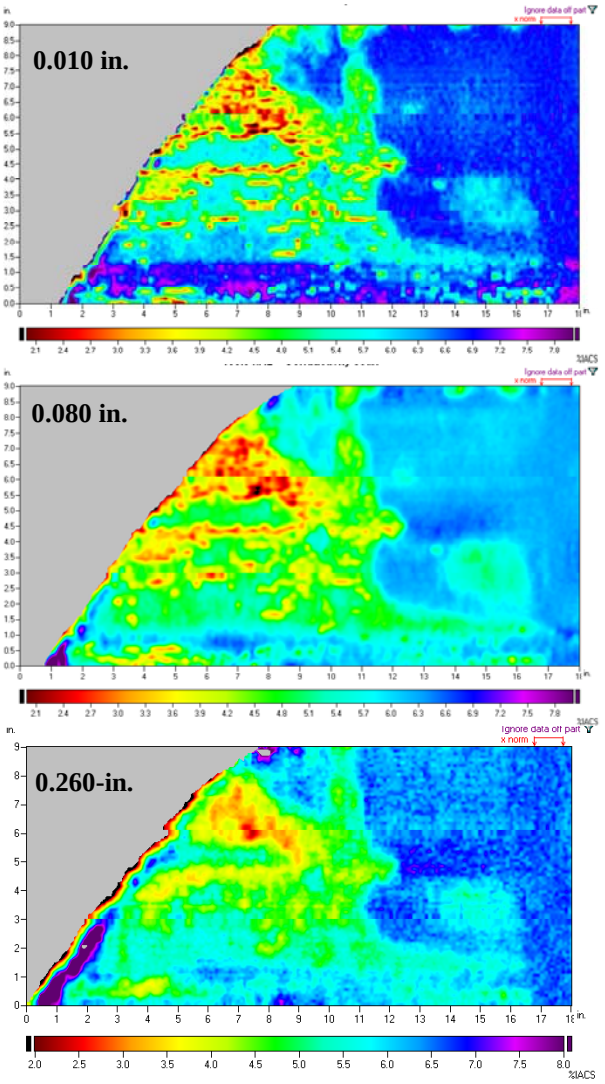

Figure 24. Effective conductivity images of SCC damage for a FA24 and several coating thicknesses.

JENTEK's MWM-Array technology enables many benefits over the existing Magnetic Particle Inspection (MPI) technology, including automatic determination of crack length and crack interaction, electronic storage and retrieval of measurement data, ability to perform at least preliminary inspection of the pipeline without having to remove the coating, and reduced surface cleaning and post inspection cleaning requirements. Figure 26 shows that the eddy-current images can provide details of cracks that are comparable to photographs of the cracks. Recently, JENTEK demonstrated this capability in the field on a TransCanada pipeline section, with support from Applus/RTD. We expect this to be a fully approved process, as an MPI replacement, within the next year. Also, a Probability of Detection (POD) study was completed on numerous SCC cracks by RTD (and JENTEK) with favorable results, strongly supporting the MWM-Array capability to replace MPI. [8]

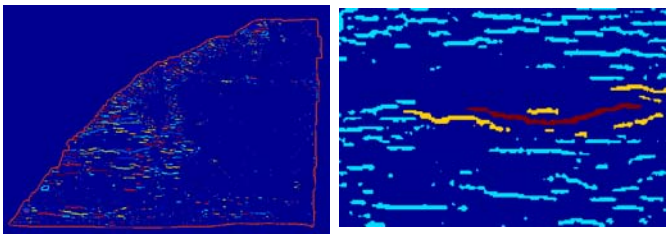

Figure 25. (Left) Each color corresponds to a crack that meets the connectivity algorithm's definition of a discrete crack. (Right) Cracks shown in yellow are those that meet the criteria for "interacting cracks" with the crack shown in brown.

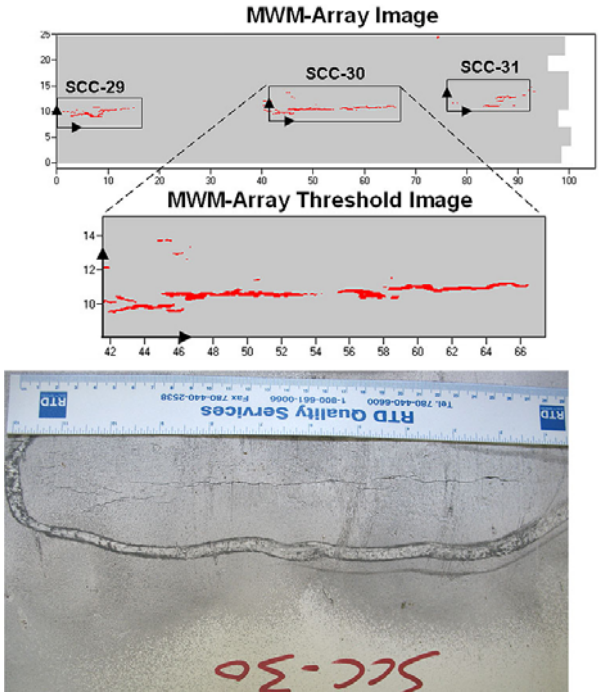

Figure 26. (Upper, Middle) MWM-Array two-color images for a pipeline section having SCC damage. (Lower) The MWM-Array images provide crack surface dimensions that are comparable to the visible cracks.

DISCUSSION

Eddy current technology is widely used in the aerospace industry and is seeing increasing use in petrochemical applications because eddy current sensor arrays permit rapid and reliable imaging of pipeline material condition. The emphasis of this paper was on inspection through coatings, but the methods can also be applied to inspections with coatings removed. Both with and without coatings, these methods can

provide information about the material condition that can assist with characterization of damage conditions and support assessment decisions.

Although a wide variety of coatings are used throughout the oil and gas industry, the sensor design and operating conditions can be adjusted to accommodate the different inspection requirements. For example, although the coating material can vary depending upon the application, such as FBE, coal tar, or some other polymeric material, these coatings are typically electrically insulating. The only property of an insulating coating that affects the eddy current response is the coating thickness. To inspect through this coating, a sensor design with a geometry (e.g., spatial wavelength) that is comparable to the thickness should be used. Selection of a sensor with a geometry that is too small would not be able to inspect through the coating and selection of a sensor with a geometry that is too large would have reduced sensitivity to the presence of small features. Similarly, the operating frequency of the instrumentation can be adjusted to accommodate different inspection requirements. Since the induced eddy current density varies with the excitation frequency and is largest on the steel surface nearest the sensor, high excitation frequencies are typically used for near-surface damage inspections. For inspections through the steel wall, for example for internal corrosion damage with an external inspection, low excitation frequencies are required.

This paper reviewed several applications for eddy current inspection from outside the pipeline. For several no coating, very thin and thin coating applications, including imaging of external corrosion, mechanical damage, and SCC, the technology is mature with capabilities demonstrated. For some applications, such as external corrosion and mechanical damage inspection through moderate thickness coatings (up to 1.0 or 1.5-in.), feasibility has been demonstrated but ongoing work is aimed at improving the inspection capability and refining equipment, such as improved scanner designs to facilitate field-level inspections. For other applications, such as external corrosion inspection through thick coatings, assessment of stresses and damage condition within mechanical damage sites, far-surface corrosion inspection, and SCC depth estimation, ongoing work is aimed at extending capabilities to address these needs. For example, for inspection through weather jackets and for through-thickness material loss estimates in steel, very low frequency (< 100 Hz) instrumentation is required.

While the emphasis of this paper was on external inspection through coatings and insulation, the same basic technology can also be applied to in-line inspection (ILI) applications with suitable hardware modifications to integrate with an ILI platform. For example, the increasing use of coatings and liners in harsh productive environments requires NDE techniques that can inspect through these barrier layers for damage, such as both internal and external corrosion. From inside the pipeline, the detection of internal corrosion through a liner is analogous to the inspection of external corrosion through a coating or insulation from outside the pipeline.

ACKNOWLEDGMENTS

The authors would like to thank the U.S. Department of Transportation (DOT), Chevron Corporation, Applus/RTD and PRCI for their support and access to relevant specimens. All conclusions are those of the authors and not the sponsoring agencies.

REFERENCES

1. N. Goldfine, V. Zilberstein, T. Lovett, “Pipeline & Piping Damage Mapping and Tracking using High-Resolution Imaging MWM-Arrays,” ASNT International Chemical and Petroleum Industry Inspection Technology (ICPIIT) X Conference, Houston, TX, June 20-23, 2007.

2. N. Goldfine, “Magnetometers for Improved Materials Characterization in Aerospace Applications,” *Materials Evaluation*, Volume 51, No. 3, March 1993.

3. N. Goldfine and D. Clark, “Introduction to the Meandering Winding Magnetometer (MWM) and the Grid Measurement Approach,” SPIE NDE Techniques for Aging Infrastructure and Manufacturing, Scottsdale, Arizona; Dec., 1996. SPIE Proceedings, Vol. 2944, 1996. pp186-192.

4. N. Goldfine, et al., “Surface Mounted Periodic Field Current Sensors for Structural Health Monitoring,” SPIE, Smart Structures and Materials NDE for Health Monitoring and Diagnostics, Newport Beach, California; March 2001.

5. N. Goldfine, V. Zilberstein, A. Washabaugh, D. Schlicker, I. Shay, D. Grundy, “Eddy Current Sensor Networks for Aircraft Fatigue Monitoring,” *Materials Evaluation*, Volume 61, No. 7, July 2003, pp. 852-859.

6. U.S. Patent Nos. 5,453,689, 5,629,621, 5,793,206, 5,966,011, RE39,206, 6,784,662, 7,049,811, 7,385,392, 7,467,057, and pending patents.

7. N. Goldfine, Y. Sheiretov, D. Schlicker, A. Washabaugh, “Rapid, Nonlinear “System” Identification for NDT, Using Sensor Response Databases,” *Materials Evaluation*, Vol. 66, No. 7, July 2008.

8. N. Goldfine, A. Washabaugh M. Windoloski, V. Zilberstein, “Replacing magnetic particle and liquid penetrant inspections with high resolution MWM-Array eddy current imaging,” ASM AeroMat Conference and Exposition, Baltimore, MD; June 26-27, 2007.

